Published in final edited form as:
Conf Proc IEEE Eng Med Biol Soc. 2014 August ; 2014: 6864–6867. doi:10.1109/EMBC.2014.6945205.

Human Eye Phantom for Developing Computer and Robot-Assisted Epiretinal Membrane Peeling*

Amrita Gupta [Student Member, IEEE],
CISST ERC at The Johns Hopkins University, Baltimore, MD 21218 USA

Berk Gonenc [Student Member, IEEE],
CISST ERC at The Johns Hopkins University, Baltimore, MD 21218 USA

Marcin Balicki [Student Member, IEEE],
CISST ERC at The Johns Hopkins University, Baltimore, MD 21218 USA

Kevin Olds [Student Member, IEEE],
CISST ERC at The Johns Hopkins University, Baltimore, MD 21218 USA

James Handa,
Wilmer Eye Institute at The Johns Hopkins School of Medicine, Baltimore, MD 21287 USA

Peter Gehlbach [Member, IEEE],
Wilmer Eye Institute at The Johns Hopkins School of Medicine, Baltimore, MD 21287 USA

Russell H. Taylor [Fellow, IEEE], and
CISST ERC at The Johns Hopkins University, Baltimore, MD 21218 USA

Iulian Iordachita [Senior Member, IEEE]
CISST ERC at The Johns Hopkins University, Baltimore, MD 21218 USA

Abstract

A number of technologies are being developed to facilitate key intraoperative actions in vitreoretinal microsurgery. There is a need for cost-effective, reusable benchtop eye phantoms to enable frequent evaluation of these developments. In this study, we describe an artificial eye phantom for developing intraocular imaging and force-sensing tools. We test four candidate materials for simulating epiretinal membranes using a handheld tremor-canceling micromanipulator with force-sensing micro-forceps tip and demonstrate peeling forces comparable to those encountered in clinical practice.

I. Introduction

Vitreoretinal microsurgery is a treatment option for a number of vision-threatening conditions, including but not limited to retinal detachment, macular pucker, and macular

*Research supported in part by the National Institutes of Health under R01 EB007969, and R01 EB000526, and in part by Johns Hopkins University internal funds.

(Corresponding author: Berk Gonenc, phone: 360-975-1676; bgonenc1@jhu.edu)..
(agupta47@jhu.edu, marcin@jhu.edu, kolds1@jhu.edu, rht@jhu.edu, iordachita@jhu.edu, jthanda@jhmi.edu, pgelbach@jhmi.edu)

holes. However, the procedure can be challenging for the surgeon due to certain intrinsic aspects of the operation. Retinal tissues are susceptible to light-induced damage and physical damage that is exacerbated by the risk of injury related to surgeon's hand tremor or unintended movements, surgical error as well as patient movement. Furthermore, the curved geometry of the eye can impede accessibility and intraocular imaging, and this, combined with the restricted intraoperative view, can hamper the detection and manipulation of delicate structures, such as epiretinal membranes (ERM) and blood vessels.

In view of the many challenges associated with vitreoretinal microsurgery, various technologies are being developed to facilitate key intraoperative actions. Developments include 3D visualization systems and robust algorithms for tracking the relative motion of the retina and surgical tools [1-3] and for delineating blood vessels. These features would help provide real-time visual feedback during surgery that can additionally be used to generate virtual fixtures with assistive robots [4]. Cooperatively-controlled robotic assistants can remove physiological hand tremor and reduce the risk of damage to the eye. Surgical tools equipped with force sensors coupled with haptic or auditory feedback could help monitor the forces applied to intraocular tissues in surgery [5]. Intraocular optical coherence tomography (OCT) is being actively investigated for its potential to provide real-time in-vivo cross-sectional information to complement the retinal surface visualization [6].

In order for these developing technologies to progress towards clinical application, they must be continuously tested in a realistic, accessible and repeatable surgical setup. Ex-vivo porcine and bovine phantoms have been used for testing purposes, but their utility is limited to a few hours before the ocular tissue properties begin to change. Animal trials are costly, time-consuming and cannot be for rapid iteration testing. Current animal models of ERM are better models of proliferative vitreoretinopathy than idiopathic macular pucker or ERM. The use of organic tissue phantoms requires biosafety training and precautionary measures, and introduces variability due to anatomical differences between samples. Therefore, there exists a great need for an artificial eye phantom for benchtop experiments that imitates key features and properties of the human eye.

A number of research groups have designed eye models for assessing new devices for ophthalmological procedures and for use as training aids for surgery. Eye phantoms simulating the optical properties of ocular tissues have been developed to evaluate spectroscopic retinal imaging and retinal OCT resolution [7-10]. Laser scanning has been used to reproduce volumetric retinal morphology for use with intraocular OCT [11]. Anatomical models of human eye geometry serve as a basis for the design of intraocular lenses [12, 13]. Iyer and Han developed an ERM phantom using a commercially available model eye [14].

The development of a microsurgical assistant system for retinal surgery at the Johns Hopkins University has created the need for an eye phantom that combines several features such as ocular geometry, fundus appearance [1-3,5], and realistic ERM peeling behavior, including forces that simulate those encountered during surgery [21]. In this paper, we present an adaptable eye phantom as well as a quantitative assessment of the forces

produced during delamination of membranes prepared from four candidate materials for simulating ERM peeling, a standard vitreoretinal microsurgical procedure.

II. Phantom Fabrication

The eye phantom comprises a water-filled soft silicone rubber sclera body containing a retina insert (Fig. 1.a). The pupil opening was delineated by a silicone O-ring (AS568A-111; ~12 mm inner diameter & ~16 mm outer diameter) into which a disposable direct imaging plano-concave contact lens (20 Degree Flat Vitrectomy Lens 1284.DD; Dutch Ophthalmic USA) was inserted with the flat side facing the retina. The external side of the contact lens was covered with an iris piece to create a pupil of diameter ~6 mm comparable to that of 3-9 mm in the human eye.

A. Sclera Body

The sclera body was cast by combining SORTA-Clear 18 parts A and B as specified ("SORTA-Clear 18"; Smooth-On, USA), along with 4 to 5 drops of white silicone pigment ("White Silicone Pigment"; Smooth-On, USA). This mixture was placed in a vacuum chamber for 5 minutes to remove any bubbles created during mixing. The mixture was allowed to set in the scleral mold for 24 hours. The resulting silicone sclera had a slightly asymmetrically positioned spherical cavity of ~25 mm inner diameter. The sclera was 1-2 mm thick on the anterior side of the eye with a ~14 mm diameter circular hole into which a 12 mm ID O-ring was bonded with silicone glue. Two standard surgical trocars inserted through the sclera act as ports for the light pipe and the surgical instrument (Fig. 1.b).

B. Retina Insert

A ¾" stainless steel ball bearing was used to cast the retina insert by dipping in clear latex paint ("Latex Paint Base"; The Monster Makers Co.). The paint was allowed to dry completely before repeating this process for a second clear layer. The retinal vasculature was hand-drawn and allowed to dry overnight before further latex paint layers were added. The subsequent layers were added with pigmented latex paint until the retina insert was 0.5 - 1 mm thick. Once dried, it was removed from the mold and inverted.

C. Epiretinal Membrane

We performed an exhaustive search for materials to simulate ERM on the retina surface. These were: 1) Liquid bandage [1] (CVS Pharmacy brand) was used as a control sample by applying a thin layer to the retina surface and allowing it to dry for 1 hour. However, unlike real ERM, the liquid bandage has a shiny appearance that causes disruptive bright reflective regions in fundus images and OCT scans. 2) Directing a controlled and focused air flow gently on the liquid bandage as it dries creates an irregular surface that produces diffuse reflection and a dull appearance. 3) Another modified liquid bandage sample is prepared with scattering particles by mixing 0.015 g of cornstarch per 0.2 mL of liquid bandage to give a matte effect. 4) The final ERM candidate is prepared by stretching Parafilm M® All Purpose Laboratory Film (Bemis Company, Inc.) until it attains a thickness of 0.08-0.09 mm, placing it on the latex surface and applying light even pressure.

D. Iris

A copper iris prototype was used to cast a mold for the iris out of soft silicone mold rubber (SORTA-Clear 18). To cast the silicone iris, the mold is sprayed with a mold release agent and filled with SORTA-Clear containing a small amount of black pigment. After 5 minutes, the solidified iris is carefully extracted.

III. Validation

A. Eyeball Phantom

The fabricated eye phantom was placed in a Delrin® plastic socket (30 mm inner diameter) coated with methylcellulose jelly that rests in a modified Sawbones (Pacific Research Laboratories, Inc.) foam skull model affixed to an adjustable acrylic platform (Fig. 1.b). The methylcellulose jelly allows the phantom to swivel within the socket with a similar range of rotation and resistance to an in vivo eyeball, while keeping it in the socket through adhesion. This setup reproduces the limited exposure available during ocular surgery, while the phantom itself replicates the geometry of the human eye sufficiently to simulate vitreoretinal microsurgery maneuvers (Fig. 1.c). The inner eye cavity diameter of 25 mm approximates a normal human eye axial length of ~24.6 mm [15]. The phantom can also be filled with water, an important requirement for intraocular imaging.

B. Epiretinal Membrane

1) Experimental Setup—In order to evaluate the mechanical properties of the candidate ERM materials, peeling tests were conducted on the setup shown in Fig. 2. Liquid bandage, its variants, and Parafilm were tested. The modifications made to liquid bandage not only affect its appearance but also change its mechanical properties. Furthermore, these materials exhibit different adhesion characteristics on different surfaces, which significantly influences the peeling behavior. For this reason, a total of four different material preparations (liquid bandage, liquid bandage with blow drying, liquid bandage with corn starch, and Parafilm) were applied on two types of base material: aluminum and latex. Aluminum is potentially useful as an electrically conductive layer for detecting contact with the simulated retina surface during peeling experiments similar to those in [20]. In the current experiments, the base surfaces were flat in order to facilitate conducting a large number of tests. Upon application, the candidate materials were sliced into 2 mm wide strips forming 10 simulated membranes per case. As the peeling instrument, a handheld tremor-canceling micromanipulator, known as Micron, was used with a force-sensing micro-forceps tip. This instrument is able to cancel undesired tremulous motion in real time via optical tracking [4]. The force-sensing forceps provide force feedback to the operator via auditory-sensory substitution [20]. During the tests, the strips were peeled off the surface with the goal of keeping the forces below 7.5 mN and the peeling speed around 0.5 mm/s, which are the approximate safety thresholds to avoid complications (such as retinal tears, detachments, hemorrhage) in rabbit retina [16,17,21]. While delaminating the simulated membranes, applied forces, and tool tip speed were recorded. After each peel, the thickness of the peeled material was also measured with a micrometer screw gauge.

2) Results and Discussion—The forces measured while delaminating each membrane type on latex and aluminum bases are shown in Fig. 3. Ten peeling trials per case were done except for liquid bandage with blow-drying and Parafilm on aluminum base, where the membrane strips were too brittle and broke off frequently, and the membrane strips did not adhere to the base, respectively. In statistical analyses, only the continuous delaminating periods were considered. Related peeling speed and material thickness values are presented in Table I.

Peeling liquid bandage off the latex base requires an average force of 7.66 mN at an average peeling speed of 0.70 mm/s. On aluminum base, the mean peeling force for similar peeling speed (0.77 mm/s) and material thickness (0.03 mm) is much lower, 4.11 mN, implying that liquid bandage adheres to latex better than it does to the metal. In either case, liquid bandage forms an unnatural shiny layer on the base unlike a real ERM.

Blow-drying the liquid bandage gives it a more realistic appearance, but makes it more brittle, which can be an issue when peeling very thin layers. The quickly blow-dried liquid bandage does not adhere to the latex surface as strongly as the normal liquid bandage does. This causes a reduction in the overall peeling force, which is about 4.58 mN for the 10 trials shown. In addition, blow-drying causes liquid bandage to dry faster and spread less on latex before it solidifies. This results in an increased overall material thickness of 0.04 mm. At this thickness, the bandage strips can still be peeled off the latex base successfully despite the brittle material properties. On aluminum base, however, we observe a completely different impact on peeling characteristics. Blowing on the liquid bandage spreads it very uniformly on the metal surface as a thin layer (0.02 mm) and causes it to stick on the base very strongly. For this reason, large forces are required for peeling (mean force in the trials shown is around 9.84 mN). Since the material is very thin and the applied forces are large, the sample strips break frequently during trials. High peeling forces and low ductility characteristics deteriorate the realistic feeling and undermine the use of blow dried liquid bandage on a metal base as a suitable surrogate for ERM.

Similar to blow-drying, adding cornstarch to liquid bandage also improves its appearance under the microscope. However, it increases the viscosity as well, leading to thicker membrane layers on both latex and aluminum surfaces (0.05 mm and 0.04 mm respectively). Mixing with cornstarch lowers the adhesive forces of the liquid bandage, and thus the average peeling forces are smaller on both base types compared to previous phantoms. As with pure liquid bandage trials, the peeling forces observed on the aluminum base are lower than those on latex.

Parafilm gives a very realistic look on latex base, and is very easy to apply. The resulting layer is much thicker (0.08-0.09 mm) than the aforementioned phantoms. Delaminating Parafilm off the aluminum base significantly lowers the adhesive forces with rare and seemingly random rises as shown in Fig. 3. This is because Parafilm does not stick well on a flat metal surface, and thus is not appropriate for simulating ERM on such a base. However on latex base, the measured peeling forces are similar to the forces observed for blow-dried liquid bandage. As opposed to blow-dried liquid bandage, Parafilm is highly ductile and does not break off easily during trials. The characteristics also match the speed and force

levels in actual surgical procedures. However, these characteristics depend on how much the Parafilm sheet is stretched before application on the surface, and thus need to be standardized to produce identical phantoms for repeatable experiments.

IV. Conclusion

In this paper we have presented a reusable, cost-effective artificial eye phantom with ERM and quantified the forces encountered during membrane delamination. Parafilm was identified as having peeling forces below the critical threshold of 7.5 mN as well as a realistic appearance against a latex base. Blow-drying and adding cornstarch to liquid bandage also reduced the adhesion to latex but also resulted in undesirable brittleness or viscosity that detracted from the use of these materials to simulate ERMs. The Parafilm membranes were much thicker than the liquid bandage variants, but were comparable in thickness to the average ERM thickness of ~0.061 mm [18]. For better use of the phantom in evaluating micro-force sensing tools [19], the large variance in Parafilm membrane thickness must be addressed and its effect in peeling properties must be analyzed to help select a standardized thickness. Additionally, constant speed peeling experiments will provide a clearer comparison of delamination forces.

To simulate typical visual access in this work, we used a readily available lens. If the eyeball is filled with water, this part, together with the O-ring, provides the necessary seal to keep fluid inside. Studies on different lens configurations are underway to better replicate the combined optics of the cornea, lens and contact lens. Our future studies aim to extend our experiments while using the tested membranes inside the eye phantom, characterize the delamination behavior in water, and add functionality for additional vitreoretinal surgery procedures, such as intra-ocular OCT and visual tracking.

References

1. Sznitman R, Richa R, Taylor RH, Jedynak B, Hager GD. Unified detection and tracking of instruments during retinal microsurgery. Pattern Analysis and Machine Intelligence, IEEE Transactions on. May; 2013 35(5):1263–1273.
2. Richa R, Balicki M, Meisner E, Sznitman R, Taylor R, Hager G. Visual tracking of surgical tools for proximity detection in retinal surgery. Proc. Information Processing in Computer Assisted Interventions (IPCAI '11). 2011; 6689:55–66.
3. Richa R, Balicki M, Sznitman R, Meisner E, Taylor RH, Hager GD. Vision-based proximity detection in retinal surgery. Biomedical Engineering IEEE Transactions on. Aug; 2012 59(8):2291–2301.
4. Becker BC, MacLachlan RA, Hager GD, Riviere CN. Handheld micromanipulation with vision-based virtual fixtures. Proc. IEEE Int. Conf. on Robotics and Automation (ICRA '11). 2011:4127–4132.
5. Gonenc B, Balicki MA, Handa J, Gehlbach P, Riviere CN, Taylor RH, Iordachita I. Preliminary evaluation of a micro-force sensing handheld robot for vitreoretinal surgery. Proc. IEEE Int. Conf. on Intelligent Robots and Systems (IROS '12). 2012:4125–4130.
6. Balicki M, Richa R, Vagvolgy B, Handa J, Gehlbach P, Taylor R. Interactive OCT annotation and visualization system for vitreoretinal surgery. AE-CAI Workshop of Medical Image Computing and Computer-Assisted Intervention (MICCAI '12). 2012
7. Lemaillet P, Ramella-Roman JC. Dynamic eye phantom for retinal oximetry measurements. J. Biomed. Opt. Nov 1-6.2009 14(6):064008. [PubMed: 20059246]

8. Corcoran AT, Muyo G, Hemert JI, Harvey AR. Development of a Widefield Phantom Eye for Retinal Optical Coherence Tomography). Proc. of SPIE. Mar 1-4.2014 8945:89450F.
9. Zawadzki RJ. Developments of a Corneal Tissue Phantom for Anterior Chamber Optical Coherence Tomography (AC-OCT). Proc. of SPIE. Feb 1-9.2013 8583:858301.
10. Agrawal A, Connors M, Beylin A, Liang C, Barton D, Chen Y, Drezek R, Pfefer T. Characterizing the point spread function of retinal OCT devices with a model eye-based phantom. Biomed. Opt. Express. May.2012 3:1116–1126. [PubMed: 22567601]
11. Zawadzki RJ, Rowe TS, Fuller AR, Hamann B, Werner JS. Toward building an anatomically correct solid eye model with volumetric representation of retinal morphology. Proc. SPIE. 2010; 7550:75502F, 1–7.
12. Brezna W, Dragostinoff DN, Prinz M. Human eye modeling for intraocular lens design and for calculating intraocular lens power. Biological and Medical Systems. 2012; 8(1):534–539.
13. Lotmar W. Theoretical eye model with aspherics. JOSA. Nov; 1971 61(11):1522–1529.
14. Iyer MN, Han DP. An eye model for practicing vitreoretinal membrane peeling. Archives of Ophthalmology. 2006; 124(1):108–110. [PubMed: 16401792]
15. Singh KD, Logan NS, Gilmartin B. Three-dimensional modeling of the human eye based on magnetic resonance imaging. Investigative Ophthalmology & Visual Science. Jun; 2006 47(6): 2272–2279. [PubMed: 16723434]
16. Gupta P, Jensen P, de Juan E. Surgical forces and tactile perception during retinal microsurgery. Proc. MICCAI. 1999; 99:1218–1225.
17. Sjaarda RN, Glaser BM, Thompson JT, Murphy RP, Hanham A. Distribution of iatrogenic retinal breaks in macular hole surgery. Ophthalmology. Sep; 1995 102(9):1387–1392. [PubMed: 9097778]
18. Wilkins JR, Puliafito CA, Hee MR, Duker JS, Reichel E, Coker JG, Schuman JS, Swanson EA, Fujimoto JG. Characterization of epiretinal membranes using optical coherence tomography. Ophthalmology. Dec; 1996 103(12):2142–2151. [PubMed: 9003350]
19. Gonenc B, Handa J, Gehlbach P, Taylor RH, Iordachita I. Design of 3-DOF Force Sensing Micro-Forceps for Robot Assisted Vitreoretinal Surgery. Proc. International Conference of the IEEE EMBS (EMBC '13). 2013:5686–5689.
20. Gonenc B, Feldman E, Gehlbach P, Handa J, Taylor RH, Iordachita I. Towards Robot-Assisted Vitreoretinal Surgery: Force-Sensing Micro-Forceps Integrated with a Handheld Micromanipulator. Proc. IEEE Int. Conf. on Robotics and Automation (ICRA '14). 2014:1399–1404.
21. Sunshine S, Balicki M, He X, Olds K, Kang J, Gehlbach P, Taylor R, Iordachita I, Handa J. A Force-sensing Microsurgical Instrument That Detects Forces Below Human Tactile Sensation. Retina. Jan.2013 33-1:200–206. [PubMed: 22810149]

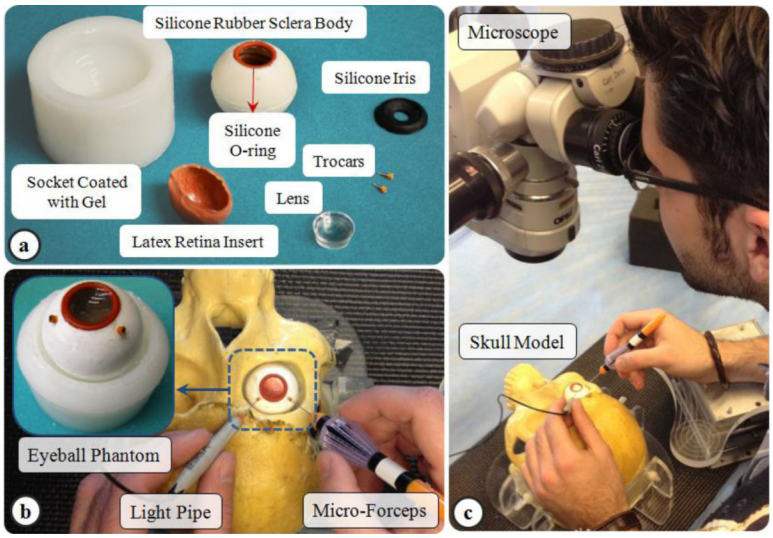

Figure 1.

Component parts of the eyeball phantom designed for bench simulations of computer-assisted ophthalmic procedures. The fabricated eye phantom was placed in a Delrin® plastic socket coated with methylcellulose jelly that rests in a skull model. The phantom replicates the geometry of the human eye sufficiently to simulate vitreoretinal microsurgery maneuvers.

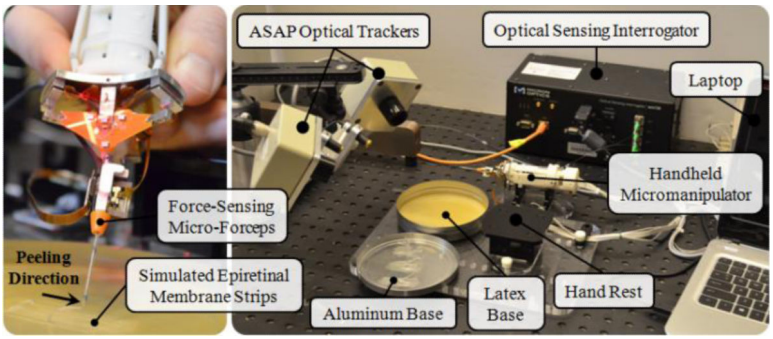

Figure 2.

Experimental setup for simulated ERM peeling using a handheld micromanipulator, Micron (left). Micron assists the procedure by providing a tremor-free tool motion, while the exerted peeling forces are sensed via the optical fibers located on the micro-forceps tip. Four different materials (liquid bandage, liquid bandage with blow drying, liquid bandage with corn starch, and Parafilm) were applied on two types of base material: aluminum and latex.

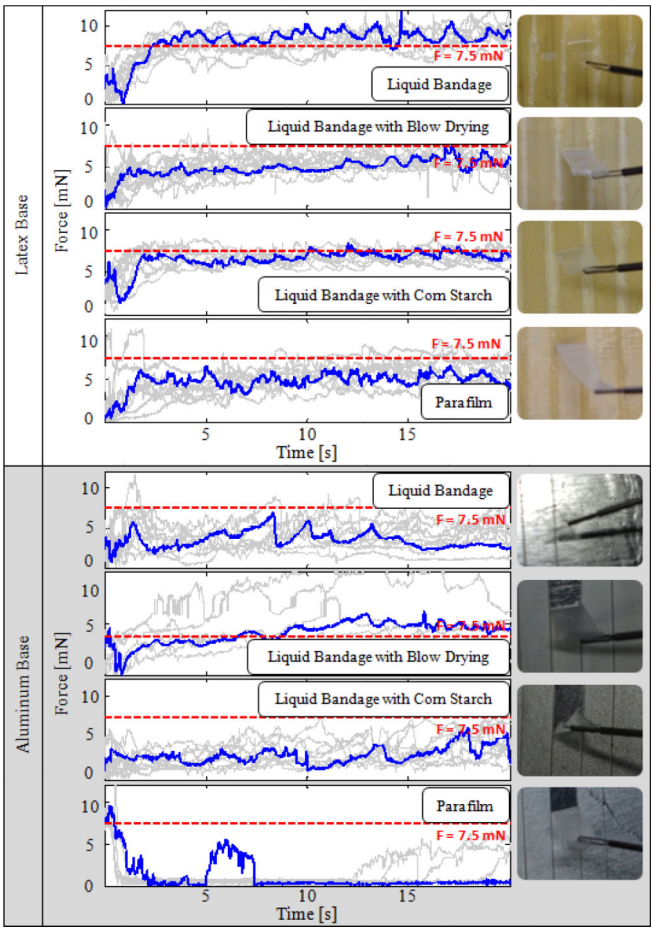

Figure 3.

Appearance of the candidate ERM materials and corresponding delamination forces on latex and aluminum bases. A representative trial is highlighted in blue in each case.

TABLE I

Delamination Properties of Erm Materials

Base	Epiretinal Membrane Material	Force [mN]		Speed [mm/s]		Thickness [mm]	
		Mean	Std. Dev.	Mean	Std. Dev.	Mean	Std. Dev.
Latex	Liquid Bandage	7.66	1.14	0.70	0.14	0.02	0.004
	Liquid Bandage with Blow Drying	4.58	1.06	0.72	0.12	0.04	0.008
	Liquid Bandage with Corn Starch	6.74	0.87	0.58	0.18	0.05	0.007
	Parafilm	5.12	1.09	0.73	0.18	0.09	0.048
Aluminum	Liquid Bandage	4.11	1.13	0.77	0.20	0.03	0.009
	Liquid Bandage with Blow Drying	9.84	4.78	0.70	0.21	0.02	0.001
	Liquid Bandage with Corn Starch	3.59	1.50	0.71	0.11	0.04	0.006
	Parafilm	1.17	0.65	1.38	0.19	0.08	0.040